MOTOR IMAGERY CLASSIFICATION USING MULTIVARIATE EMPIRICAL MODE DECOMPOSITION (MEMD) BASED FUNCTIONAL CONNECTIVITY FEATURES

by

Fatih Ekrem Onat

B.S., in Electronics & Comm. Engineering, Istanbul Technical University, 2020

Submitted to the Institute of Biomedical Engineering
in partial fulfillment of the requirements
for the degree of
Master of Science
in
Biomedical Engineering

Boğaziçi University
2023

MOTOR IMAGERY CLASSIFICATION USING MULTIVARIATE EMPIRICAL MODE DECOMPOSITION (MEMD) BASED FUNCTIONAL CONNECTIVITY FEATURES

ACKNOWLEDGMENTS

First of all, I would like to thank my advisor Prof. Dr. Ahmet Ademoğlu for his guidance and endless patience during the preparation of this thesis.The intellectual environment he had created in his laboratory has deeply influenced me for my future endeavors. I would also like to thank Asst. Prof. Görkem Serbes for his advice and support for my academic career.

Lastly, I would like to thank my mother, Prof. Dr. Handan Kamış, for raising and supporting me through the years and bringing me up to these years.

ACADEMIC ETHICS AND INTEGRITY STATEMENT

I, Fatih Ekrem Onat, hereby certify that I am aware of the Academic Ethics and Integrity Policy issued by the Council of Higher Education (YÖK) and I fully acknowledge all the consequences due to its violation by plagiarism or any other way.

Name : ______________________________ Signature: ______________________________

Date: ______________________________

ABSTRACT

MOTOR IMAGERY CLASSIFICATION USING MULTIVARIATE EMPIRICAL MODE DECOMPOSITION (MEMD) BASED FUNCTIONAL CONNECTIVITY FEATURES

Electroencephalogram (EEG) motor imagery signals are widely used for the implementation of brain-computer interfaces (BCI). Recently, functional connectivity measures have attracted attention as they can be used to capture statistical dependencies among EEG channels. However, functional connectivity during motor imagery tasks have not been fully explored. This study utilizes Instrinsic Mode Function (IMF) level phase locking value (PLV), coherence, and imaginary part of coherency in left-hand/right-hand motor imagery classification. EEG signals are decomposed into IMFs via noise-assisted multidimensional empirical mode decomposition (NA-MEMD), and connectivity metrics over the selected four channels are calculated for each trial as raw data and as a function of time and frequency. Resulting features are used to train multiple classifiers and their accuracy scores are analyzed. Best results are obtained using features derived from time-frequency functions of imaginary part of frequency where the overall accuracy score of 0.77 is achieved. This study shows that the change of connectivity throughout the duration of the task provides a more effective feature than connectivity calculated using each trial as raw data. Achieved accuracy scores are comparable to similar studies with the additional advantage of using few number of channels.

Keywords: Electroencephalogram, Brain-Computer Interface, Motor Imagery, Empirical Mode Decomposition, Functional Connectivity

ÖZET

ÇOKLU-DEĞİŞKENLİ DENEYSEL KİP AYRIŞTIRIMI-TABANLI İŞLEVSEL BAĞLANTISALLIK ÖZNİTELLİKLERİYLE MOTOR İMGELEME SINIFLANDIRMASI

Elektroensefalografi motor imgeleme sinyalleri, beyin-bilgisayar arayüzleri uygulamalarında sıklıkla kullanılmaktadır. Son zamanlarda, işlevsel bağlantısallık ölçütleri, EEG kanalları arasındaki istatistiksel bağımlılıkları yakalayabilmesi nedeniyle ilgi toplamıştır. Ancak, motor imgeleme görevleri sırasındaki işlevsel bağlantısallık henüz tam olarak keşfedilememiştir. Bu çalışmada, EEG sinyallerinden gürültü destekli çoklu boyutlu deneysel kip ayrıştırımı ile elde edilen içsel mod fonksiyonları arasında hesaplanan faz kilitleme değeri, koherans, ve koheransın sanal kısmı değerleri sağ-el/sol-el motor imgeleme sınıflandırmasında kullanılmıştır. Sonuçlar analiz edildiğinde, en iyi doğruluk skorunun koheransın sanal kısmının zaman-frekans fonksiyonlarından türetilen özellikler kullanılarak 0.77 olarak elde edildiği görülmüştür. Bu çalışma ile işlevsel bağlantısallık ölçütlerinin zamana göre değişiminin motor imgeleme sınıflandırması için işlenmemiş veriden hesaplanan değerlere kıyasla daha etkili olduğu gösterilmiştir. Bu çalışmada daha az sayıda kanal kullanılması avantajıyla benzer çalışmalarla kıyaslanabilir sonuçlar elde edilebilmiştir.

Anahtar Sözcükler: Elektroensefalogram, Beyin-Bilgisayar Arayüzü, Motor İmgeleme, Deneysel Kip Ayrıştırımı, Fonksiyonel Bağlantısallık

TABLE OF CONTENTS

LIST OF FIGURES

LIST OF TABLES

LIST OF SYMBOLS

x	Signal
e	Envelope of a Signal
m	Local Mean
d	Detail Signal
IMF_m	m_{th} Scale IMF
p^θ	Projected Signal
x^θ	Direction Vector
e^θ	Multivariate Envelope
j	Imaginary Unit
ϕ_{xy}	Phase Difference Between x and y
S_x	Power Spectral Density of x
S_{xy}	Cross Spectral Density of x and y

LIST OF ABBREVIATIONS

BCI	Brain-Computer Interfaces
EEG	Electroencephalography
ECoG	Electrocorticography
MEA	Microelectrode Array
fMRI	Functional Magnetic Resonance Imaging
SSVEP	Sinusoidal Steady State Visual Evoked Potentials
MI	Motor Imagery
EMD	Empirical Mode Decomposition
MEMD	Multivariate Empirical Mode Decomposition
NA-MEMD	Noise-Assisted Multivariate Empirical Mode Decomposition
FC	Functional Connectivity
PLV	Phase Locking Value
COH	Coherence
iCOH	Imaginary Part of Coherency
t-f	Time - Frequency
LR	Logistic Regression
SVM	Support Vector Machine
LDA	Linear Discriminant Analysis
RF	Random Forest Classifier
GBC	Gradient Boosting Classifier

1. INTRODUCTION

Brain-computer interfaces (BCIs) provide a means to restore lost or impaired motor functions by establishing a direct communications channel between the brain and an external device [1]. Both invasive recording methods, such as electrocorticography (ECoG) and microelectrode arrays (MEA), and non-invasive methods, such as electroencephalography (EEG) and functional magnetic resonance imaging (fMRI), have been studied for BCI applications. Among these methods, EEG has attracted the most attention owing to its desirable properties such as, non-invasiveness, portability, and temporal resolution [2].

EEG-based-BCIs can be implemented using various experimental paradigms such as steady-state visual evoked potentials (SSVEP), motor imagery (MI), and P300 [2]. Motor imagery involves the imagination of a movement and voluntary suppression of the movement, during which a μ/β event related synchronization phenomena can be observed around the motor cortex [2], [3]. As the generation of these signals depends entirely on the user's intent, motor imagery-based-BCIs are useful in restoring function for people with severe disabilities.

Feature extraction and classification of motor imagery EEG signals have been a focus among BCI researchers. Wavelet transform [4], common spatial patterns [5], and empirical mode decomposition (EMD) [6] have been applied for feature extraction from MI EEG signals. Among these methods EMD is an entirely data-driven and highly adaptive method and has been shown to be a capable tool for the analysis of nonlinear and non-stationary signals, such as EEG.

Functional connectivity is a measure of the correlation or synchronization between different brain regions. Measures such as correlation coefficient, phase locking value, coherence and imaginary coherence can be used to quantify functional connectivity. These measures can provide insight for the brain networks and their roles in various neural functions [7]. Functional connectivity has gained popularity in recent years and has been employed in motor imagery analysis and classification [8].

The key motivation behind this study is to utilize brain connectivity to correctly identify motor imagery tasks with a small number of channels. Currently, studies that focus on motor imagery classification with connectivity features either use a large number of channels which makes them impractical for real world applications, or achieve low accuracy that makes them unreliable. The main challenge with functional connectivity features when using only a few channels is that connections may not occur in a consistent pattern. This study uses multidimensional empirical mode decomposition (MEMD) to decompose the EEG signals in order to calculate connectivity among same-scale IMFs that have narrower frequency bands. As MEMD is a data adaptive method that decomposes a signal without imposing any restrictions on the signals, consistent connectivity patterns may be obtained in one or more IMF scales even for small number of channels.

This study focuses on extracting meaningful functional connectivity features for left-hand/right-hand motor imagery classification task. EEG signals are decomposed using MEMD and IMF-level connectivity is calculated using metrics such as PLV, coherence, and imaginary coherence. Additionally, imaginary coherence is calculated as a function of time and frequency, and statistical descriptors are extracted from the resulting functions as features. Resulting features are tested using several classifiers such as logistic regression and gradient boosting classifier.

Organization of the thesis is as follows: In Chapter 2, BCI systems and their applications are described. In Chapter 3, motor imagery is defined and recent literature on motor imagery classification is summarized. In Chapter 4, empirical mode decomposition and its variations as well as their application to motor imagery data are explained. In Chapter 5, general information on functional connectivity and various functional connectivity metrics that have been applied to motor imagery data are provided. In Chapter 6, classification results of different classifiers are given. In Chapter 7, classification results are discussed and compared with former studies in literature.

In Chapter 8, conclusions and future work are presented.

2. BRAIN COMPUTER INTERFACES

A brain-computer interface is a path of communication between the brain and an external device such as a computer or a robotic limb. A BCI system processes the electrical activity of the brain and generates control commands for a device. These systems enable people to directly interact with digital systems using signals generated by brain activity.

Electrical activity in the brain was first observed in 1920s and by measuring this activity on the scalp, the concept of EEG was conceived in 1929. EEG became a quintessential tool in analyzing brain activity and as the EEG technology grew the idea that these signal could be used to communicate with external devices emerged. In 1968, it was discovered that certain features of EEG could be consciously controlled which led to the emergence of the term "Brain-Computer Interface" in 1973. Next major advancement in BCI research was the invention of $P300$ systems in 1988. Shortly after in the early 1990s, sensorimotor rhythms were employed in BCIs leading to the definition of motor imagery-based BCIs. Also in the 1990s, slow cortical potentials were employed in systems that allowed paralyzed patients to spell letters using *neurofeedback*. In the early 2000s steady-state visual evoked potentials arose as a new paradigm for BCI systems. At the same time, it was shown that rats and monkeys could use invasive BCI systems to control robotic arms [9]. Since the beginning of the new century, both the number of studies on BCIs and their scope have greatly increased and BCI became one of the mose popular topics in neuroscience.

2.1 Types of BCI

Depending on how they are used and what the implementation method is, the BCIs can be categorized in different ways. These categorizations include; *dependent* and *independent*, *invasive* and *non-invasive*, and *synchronous* and *asynchronous* BCIs [10].

Dependent and independent BCI : One commonly made distinction in BCIs comes from the dependency to motor control. A dependent BCI requires a degree of motor control from the user. Steady-State Visual Evoked Potential (SSVEP) is an example of a dependent BCI as it requires the users to control the direction of their gaze. On the other hand, an independent BCI does not require any motor control.

Invasive and non-invasive BCI : Depending on the method used for the measurement of the brain signals, BCIs can be categorized as invasive or non-invasive. If the brain signals are measured using sensors placed within the brain this type of BCI is categorized as invasive such as *ECoG* or *Micro Electrode Array* (MEA). On the other hand, if the measurements are done from outside the brain, this type of BCI is said to be non-invasive. EEG and fMRI are examples of non-invasive methods used in BCI systems.

Synchronous and asynchronous BCI : Synchronicity is another metric that is used for the categorization of BCIs. In a synchronous BCI system, the time periods in which the user can interact with the application is determined by the system. If the application can be controlled at any time by the user the system is said to be asynchronous. By their nature, synchronous systems are more flexible and more comfortable for the user. However they are more challenging to design compared to the asynchronous systems.

2.2 BCI application areas

BCI systems are used in various fields such as medicine, entertainment and defence. Main applications of BCI in the medical field can be given as; rehabilitation, diagnosis, and treatment.

Rehabilitation : In neurorehabilitation, BCI systems are used to record and decode localized brain activity while the patient performs a motor or mental imagery task. The primary goal in these applications is to promote the activation of chosen brain areas and to aid neural plasticity [11].

Diagnosis : In diagnostic medicine, BCI systems are used for data collection and processing in order to detect anomalies. An application in this area is seizure detection where a BCI system can be employed to detect and localize epilepsy focus which can then be surgically treated [12].

Treatment : BCI in treatment is mainly used stimulate certain brain regions. A commonly used method in this area is deep brain stimulation which can be used to treat Parkinson's disease [11].

Motor imagery BCI : Motor imagery is defined as the state in which a subject imagines while carrying out a certain task. During motor imagery the subject visualizes oneself planning and performing the action while blocking the motor execution of the task [13]. Brain activity during motor imagery is related to similar categories of activity while preparing actual motor actions [14],[15]. MI presents itself as a momentary *event related desynchronization* (ERDS) in $\mu-\beta$ rhythms measured in the sensorimotor cortex [16]. By correctly detecting and classifying MI tasks in EEG, it can be utilized to build robust BCI systems.

As MI can be observed in EEG signals, portable non-invasive BCIs can be implemented at a low cost and high temporal resolution. In addition to the inherent qualities of EEG systems, MI is also advantageous compared to other EEG paradigms. Main advantage of MI is that the generation of MI response is entirely dependent of the user's intention, which means that MI can be utilized in development of independent and asynchronous BCIs. However, one difficulty in designing MI-based systems is that the activity during MI tasks is more subtle compared other EEG paradigms which makes the detection and correct classification of the tasks more challenging.

MI-based BCIs have been widely studied in the literature. Most studies focus on robust feature extraction methods for the classification of MI tasks with *SVM* and *LDA* being the most common classifiers. Commonly used methods for feature extraction includes common spatial patterns [17, 18], wavelet transform [19, 20], empirical mode decomposition [21, 22, 23]. Recently, functional connectivity and graph based classification have also became popular in EEG analysis and MI classification [24, 25].

3. METHODOLOGY

3.1 Dataset

The algorithms in this study are tested on Physionet [26] EEG Motor Movement/Imagery Dataset [27]. This dataset contains 64-channel EEG signals from 109 volunteers recorded using BCI2000 system. Experimental protocol consists of 14 experimental runs: two one-minute baseline runs, and three two-minutes runs of following movement/imagery tasks:

1. Open and close left or right hand
2. Imagine opening and closing left or right hand
3. Open and close both hands or both feet
4. Imagine opening and closing both hands or both feet

3.2 Empirical Mode Decomposition (EMD)

EMD is a data-driven time-frequency analysis method that adaptively decomposes a given signal info a finite set of oscillatory modes called intrinsic mode functions (IMF). The decomposition is done through a sifting process where each IMF satisfies following conditions: (i) the number of local extrema and the number of zero crossings can differ by at most one; (ii) the mean of the envelopes defined by the local maxima and the local minima is zero. This process is entirely data-driven meaning that no *a priori* knowledge is required and no predetermined constraints are imposed on the data [28]. Flowchart for the EMD algorithm applied to a signal $x(t)$ is given in Figure 3.1.

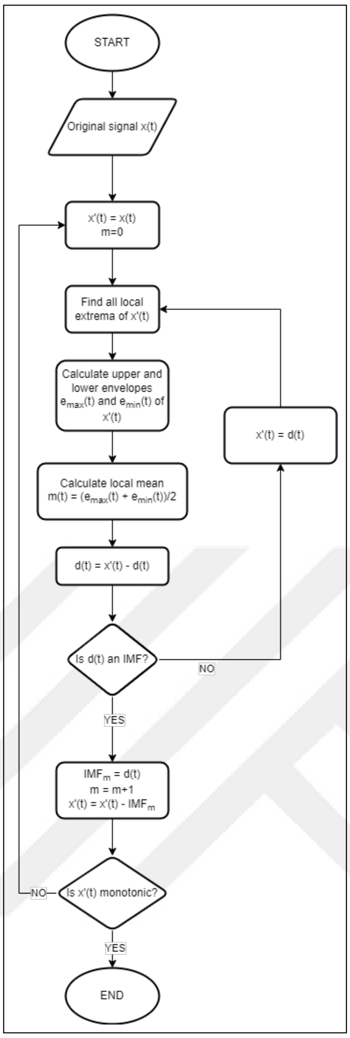

Figure 3.1 Flowchart of Empirical Mode Decomposition.

EMD has several advantages over similar signal decomposition methods. First, EMD is a completely data-driven method and IMFs obtained from the decomposition are amplitude/frequency modulated and sparse, which enables one to investigate intrinsic patterns on multiple scales without requiring *a priori* assumptions on the data. Second, EMD ensures time-frequency accuracy at instantaneous frequency level by identifying multiple within- and cross-channel scales in the signal. And third, multivariate extensions of EMD enable intrinsic, scale-dependent analyses of synchrony and causality [29].

While EMD is a robust time-frequency analysis method for single-channel signals, it has certain drawbacks when applying to multivariate data. EMD algorithm, when applied to each channel separately, may produce different number of IMFs or may cause misalignment in IMF scales. This diminishes the usability of EMD in analysis of multivariate data.

3.2.1 Multivariate Empirical Mode Decomposition (MEMD)

MEMD is a multivariate extension of the EMD algorithm that enables its application to multivariate data without issues like IMF alignment. As local extrema cannot be defined for multivariate signal, MEMD algorithm involves signal projections in an $n-$dimensional space to calculate multiple $n-$dimensional envelopes as the first step. The local mean is calculated by averaging these envelopes [30]. The algorithm for MEMD for a signal $x(t)$ is described as follows:

1. Set $x'(t) = x(t)$
2. Select a suitable pointset for sampling on an $(n-1)-$dimensional sphere.
3. Calculate the projection $p^{\theta_k}(t)|_{t=1}^{T}$ of $x'(t)$ along the direction vector x^{θ_k} for all k to obtain the set of projections $p^{\theta_k}(t)|_{k=1}^{K}$.
4. Locate time instants $t_i^{\theta_k}$ corresponding to the local maxima of the projected signals.
5. Calculate multivariate envelopes $e^{\theta_k}(t)|_{t=1}^{T}$ by interpolating the input signal.
6. Calculate the local mean $m(t)$ by averaging multivariate envelopes.
7. Extract $d(t) = x'(t) - m(t)$. If $d(t)$ satisfies the conditions valid for IMF functions, set $IMF_n = d(t)$ and $x'(t) = x'(t) - d(t)$, otherwise set $x'(t) = d(t)$ and repeat the procedure.

By applying EMD algorithm to all channels together, as opposed to applying to each channel separately, several desirable features of the MEMD algorithm can be utilized. First, as the data is analyzed in the $n-$dimensional space where they reside, joint channel properties are preserved. Second, the data channels produce the same number of IMFs that are scale-aligned. And third, MEMD algorithm enables robust multivariate $t-f$ analysis even if mode mixing occurs since IMFs of the same scale will still contain aligned composite scales [29]. The main downside of the MEMD algorithm is that mode-mixing may occur among IMFs of different scales, indicating that there may be overlap in their frequency spectra. This may cause difficulty in analyses if the desired signal resides in a certain dyadic subband [31].

3.2.2 Noise-assisted MEMD (NA-MEMD)

In order to alleviate the issues caused by mode mixing in MEMD, the algorithm has been extended to noise-assisted MEMD. In NA-MEMD, extra channels containing white Gaussian noise are added to the original signal before decomposition. This takes advantage of the quasi-dyadic filterbank property of MEMD on white noise. Noise channels are decomposed into IMFs containing a subband of the original signal. On the other hand, IMFs of the data channels are aligned based on the quasi-dyadic filterbank structure, reducing the mode-mixing problem. The number of the extra noise channels is a metric that can be optimized, although adding two extra channels is generally sufficient [31].

3.3 Functional connectivity

Functional connectivity can be defined as the statistical dependence between neuronal activation patterns of remote brain regions. Connections that are highlighted with functional connectivity analyses only mean that there is a correlation between the activity in two regions and do not imply an anatomical connection [32]. Functional connectivity analyses can be used to obtain valuable information on activation patterns during a specific task or event.

As EEG signals are measured from the electrodes placed on the scalp, electrical signals pass through tissues and bones before reaching the electrode. This may cause the activity from one region to be observed in more than one channel. This phenomena is referred to as the generally volume conduction effect. As functional connectivity metrics usually measure the degree of statistical correlation between different brain regions, volume conduction effect may cause false connections to be observed. This is an important point that must be taken into account when using functional connectivity measures [33].

3.3.1 Phase Locking Value

: Phase locking value is defined as a measure of synchronization between two signals. The formula for PLV between signals $x(t)$ and $y(t)$ in a time period T is calculated as:

$$PLV = \frac{1}{T}\left|\sum_{t=1}^{T} e^{j\phi_{xy}(t)}\right| \tag{3.1}$$

where $\phi_{xy}(t)$ is defined as the phase difference between signals $x(t)$ and $y(t)$ and it is computed using Eq. 3.2

$$\phi_{xy}(t) = \phi_x(t) - \phi_y(t) \tag{3.2}$$

Signals are said to be completely desynchronized if the PLV value is 0, and completely synchronized if the PLV value is 1 [34].

3.3.2 Coherency

Coherency is a complex valued function of frequency that is used to calculate the spectral similarity between a pair of signals. It is calculated as:

$$Coherency = \frac{S_{xy}}{\sqrt{S_x \cdot S_y}} \tag{3.3}$$

where S_{xy} is the cross spectral density of $x(t)$ and $y(t)$, and S_x, S_y are their power spectral densities, respectively. The power spectral densities are computed using Eq. 3.4, Eq. 3.5, and Eq. 3.6

$$S_x = \lim_{T \to \infty} \frac{|X(f)|^2}{T} \tag{3.4}$$

$$S_y = \lim_{T \to \infty} \frac{|Y(f)|^2}{T} \tag{3.5}$$

$$S_{xy} = \lim_{T \to \infty} \frac{X^*(f)Y(f)}{T} \tag{3.6}$$

where $X(f) = \int_{-\infty}^{\infty} e^{-i2\pi ft}x(t)dt$ and T is the length of time for the signals.

Various other connectivity metrics can be derived from coherency for further analysis. Most important metrics derived from coherency are coherence and imaginary part of coherency [35].

Coherence: Coherence is the absolute value of coherency. The magnitude of coherence gives information about the degree of correlation between two signals. Coherence is calculated as:

$$COH = |Coherency| \tag{3.7}$$

COH can take values between 0 and 1. A COH value of 0 indicates no correlation while a value of 1 indicates perfect correlation. One downside of COH is that it is insensitive to the time delay between the signals. This means COH can report strong correlation in the case of volume conduction effect which may result in false connections in the analysis [35].

Imaginary part of coherency: Another metric that is derived from coherency is the imaginary part of coherency. It is calculated as:

$$iCOH = imag(Coherency) \tag{3.8}$$

This returns 0 if there is no time lag between the signals and returns 1 if the phase difference between the signals is $\pi/2$ [35].

The main advantage of the imaginary part of coherency is that it is a robust metric against volume conduction effect. As $iCOH$ returns close to zero when there is small to none time difference between the signals, false connections caused by the volume conduction are not observed. This property makes the imaginary part of coherency a powerful measure for functional connectivity analysis.

3.4 Machine learning models and training

The extracted features are used to train various models, namely; *logistic regression classifier*, *support vector machine*, *linear discriminant analysis*, *decision tree*, and *gradient boosting classifier*. Training is done using three separate training schemes to test the usability of the features in various aspects;

1. *Subject-pooling* is used to test the general performance of the features. Here, the trials from all subjects are pooled and used to train the models with five-fold cross validation.

2. *Leave-one-subject-out scheme* is used to test the performance of the features for a subject that has not been seen by the classifier. For each subject, the data

belonging to the subject is left out as as test set and the model is trained with the data from all remaining subjects.

3. *Within-subject training* is used to test the performance of the models for the case where training and test data are obtained from the same subject. For each subject, only the data from the subject is used with five-fold cross validation to train the models.

4. APPLICATION AND RESULTS

All analyses and model training are done on a computer equipped with *NVidia GeForce RTX 3050 GPU*, *Intel Core i7-11800H CPU*, *16GB RAM*, and *512 GB* storage using *Python* programming language.

4.1 Data preprocessing

In order to minimize the number of channels, analyses are limited to FC_z, C_3, C_z, C_4 which are above the sensorimotor cortex out of the 64 channels in the dataset. Raw EEG signals from four channels are first bandpass filtered using $6-35Hz$ FIR filter. Signals are then seperated into six second epochs, -1.5s - 4.5s around the cue onset, and labeled based on the task. Epochs relating to left-hand/right-hand motor imagery are seperated for further analyses. Subjects 88, 92, and 100 are excluded from the study as the sampling frequency do not match with the rest of the subjects and no explanations on this issue is provided on dataset sheet. Bandpass filter design, and epoching is done using *MNE-Python* module [36].

4.2 MEMD

MEMD algorithm is applied to each epoch separately. As the activity related to motor imagery is usually observed in the first three IMFs, in order to keep the number of IMFs small and consistent across trials and subjects, first five IMFs are stored for further analyses. Figure 4.1 shows the first five IMFs obtained via MEMD algorithm.

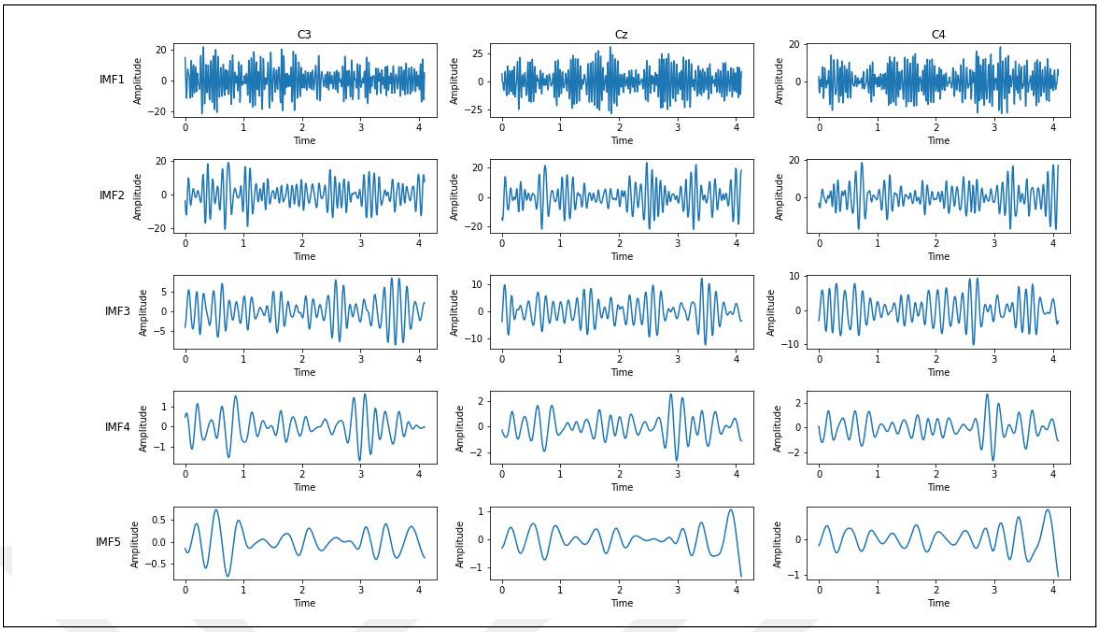

Figure 4.1 First five IMFs of left-hand motor imagery signal obtained via MEMD.

Similarly, IMFs are calculated for each epoch separately using NA-MEMD. For noise assistance, two channels of white Gaussian noise with 10% of the power of the original EEG signal are added. Figure 4.2 shows the first five IMFs obtained via MEMD algorithm.

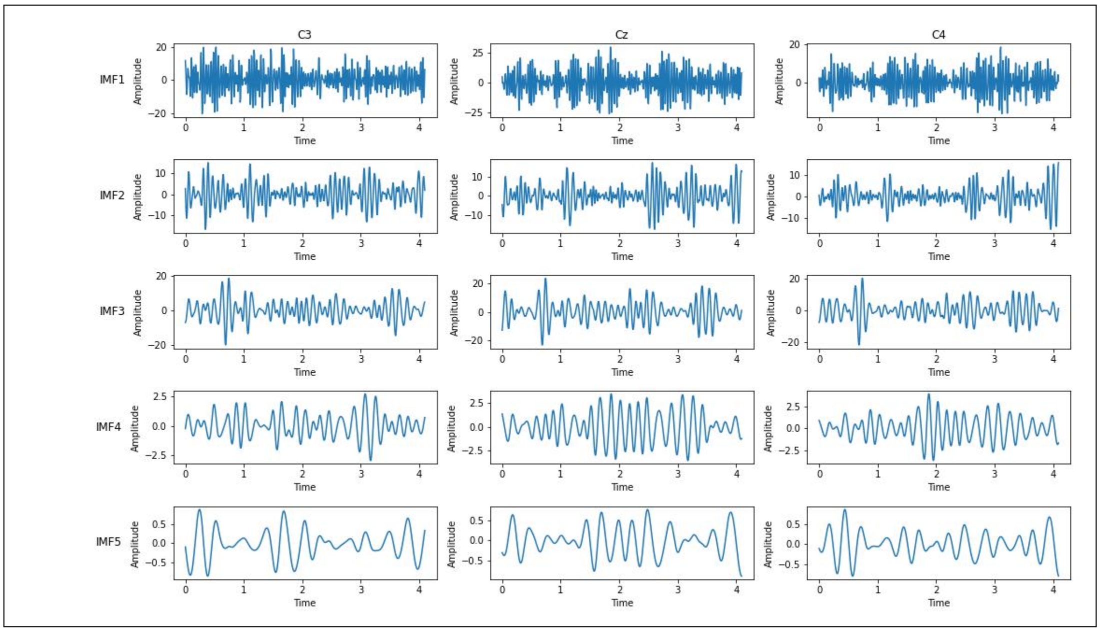

Figure 4.2 First five IMFs of left-hand motor imagery signal obtained via NA-MEMD.

The main advantage of NA-MEMD over MEMD is that the mode mixing problem, where the frequency spectra of different IMF scales overlap, is alleviated with noise assistance. Figure 4.3 compares the frequency spectra of IMFs obtained via MEMD and NA-MEMD.

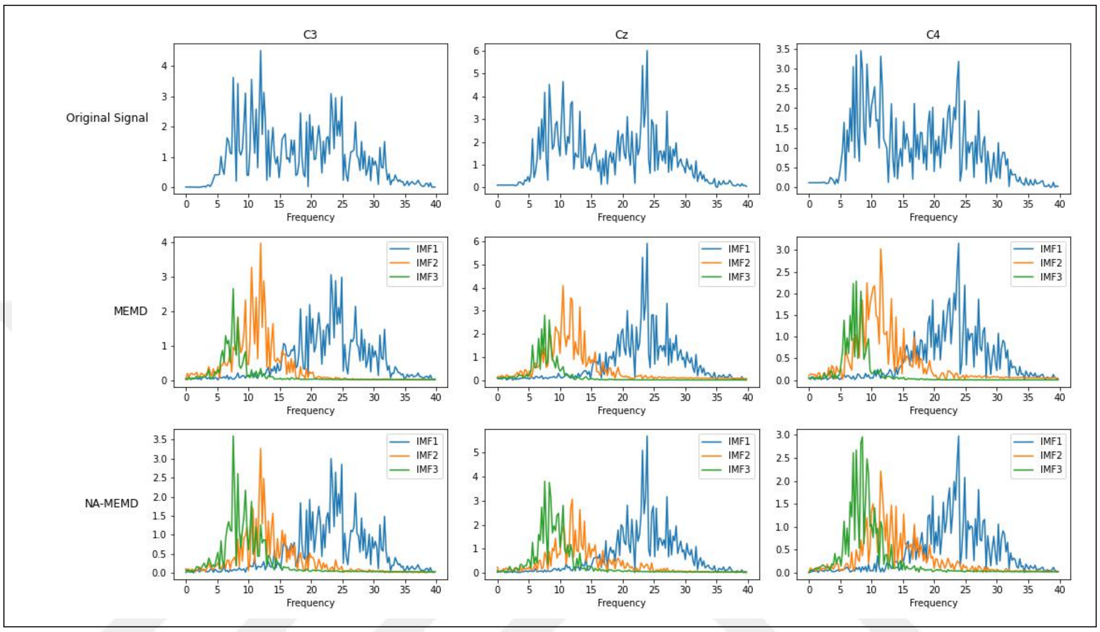

Figure 4.3 Frequency spectra of the original signal and first three IMFs obtained via MEMD and NA-MEMD.

As NA-MEMD is able to produce IMFs that have better separation in frequency, IMFs obtained via NA-MEMD are chosen for connectivity calculations. Additionally, basic statistical descriptors are calculated from IMF time series to serve as baseline for classification. Statistical descriptors used are; *mean*, *standard deviation*, *variance*, 25^{th} *quartile*, *median*, 75^{th} *quartile*, *kurtosis*, and *skewness*. Each channel produced 40 features as a result. In total, 160 features were extracted for 4533 trials.

4.3 Functional connectivity

Functional connectivity metrics are calculated between the same scale IMFs of each channel for each trial. In order to capture the connections during the task, calculations are done in the time interval 1s - 4s after cue onset.

4.3.1 PLV

Single-trial PLV values were calculated using Eq. 3.1. In total, 30 PLV features were extracted for 4533 trials. PLV values averaged across trials at each IMF level for Subject 1 for both tasks is given in Figure 4.4.

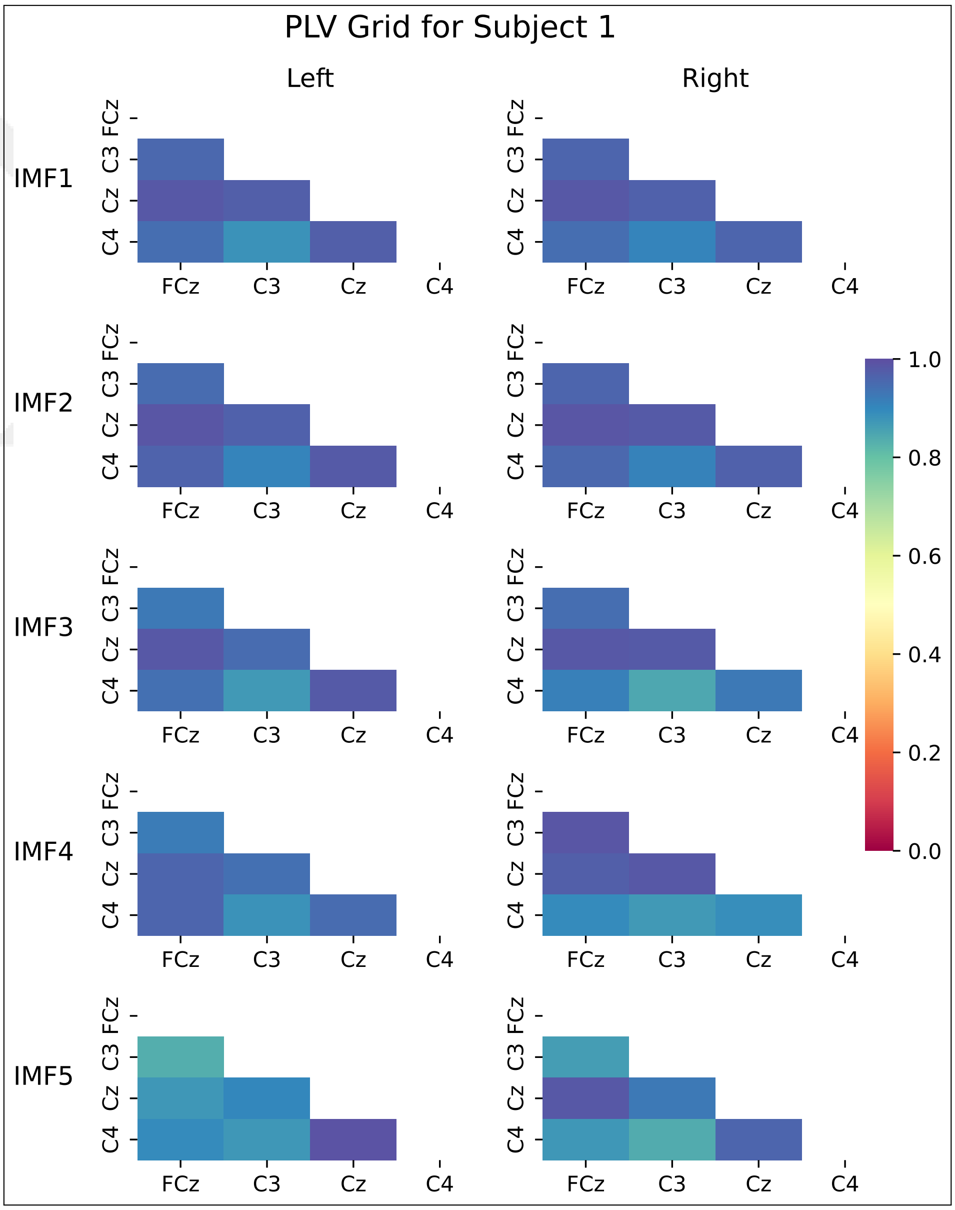

Figure 4.4 PLV between IMF scales for Subject 1.

4.3.2 Coherence

Single-trial coherence is calculated using the connectivity package in *MNE-Python* module [36]. In total, 30 COH features were extracted for 4533 trials. Trial-averaged COH values at each IMF level for Subject 1 for both tasks are given in Figure 4.5.

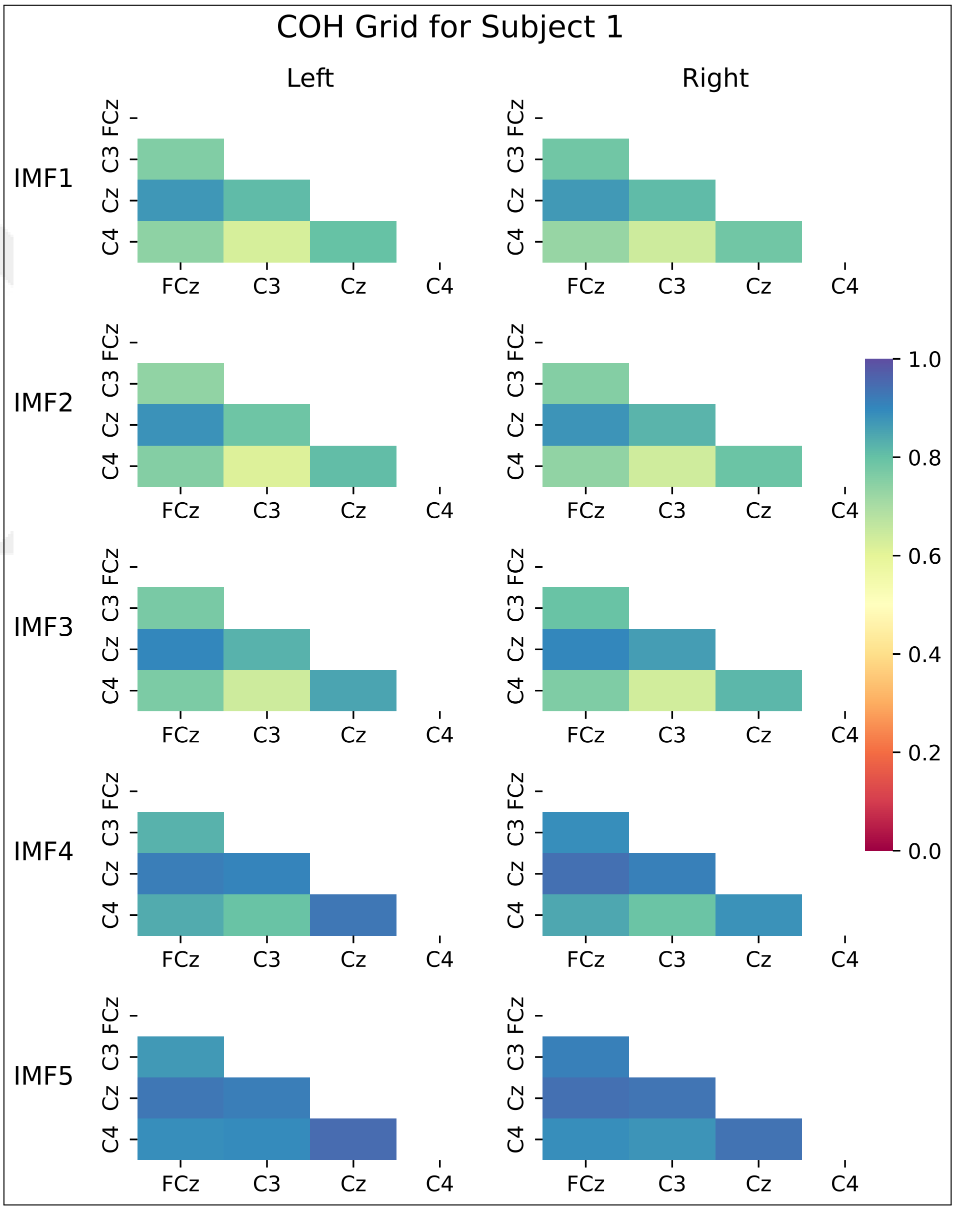

Figure 4.5 Coherence between IMF scales for Subject 1.

4.3.3 Imaginary part of coherency

Connectivity package in *MNE-Python* module is used to calculate imaginary part of coherency. Single-trial $iCOH$ is first calculated from the raw data. In total, 30 iCOH features were extracted from raw data for 4533 trials. Figure 4.6 shows the $iCOH$ values averaged across trials for Subject 1 for both tasks.

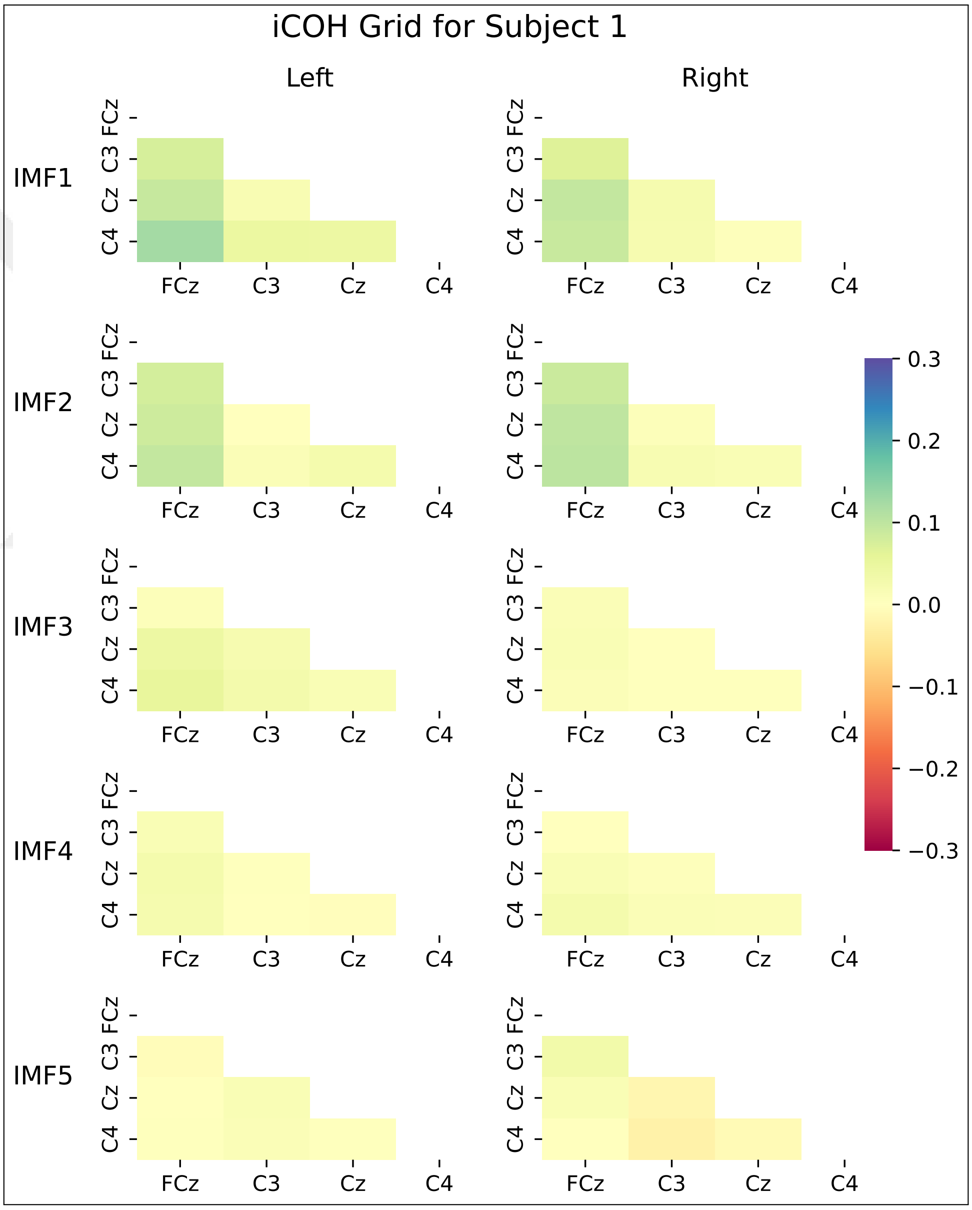

Figure 4.6 Coherence between IMF scales for Subject 1.

Additionally, $iCOH$ is also calculated as a function of time and frequency during the trial. Time-frequency function of $iCOH$ is obtained by calculating $iCOH$ in 250ms time windows with 125ms overlap through the duration of the trial. For this calculation, the time interval 0s - 4s after cue onset is used to capture initial changes in connectivity. Figure 4.7 and Figure 4.8 shows the time-frequency functions of $iCOH$ between channels FC_z-FC_3 and FC_z-FC_4. Statistical descriptors are calculated from the time-frequency functions to be used in classification. In total, 240 t-f function of iCOH features were extracted for 4533 trials.

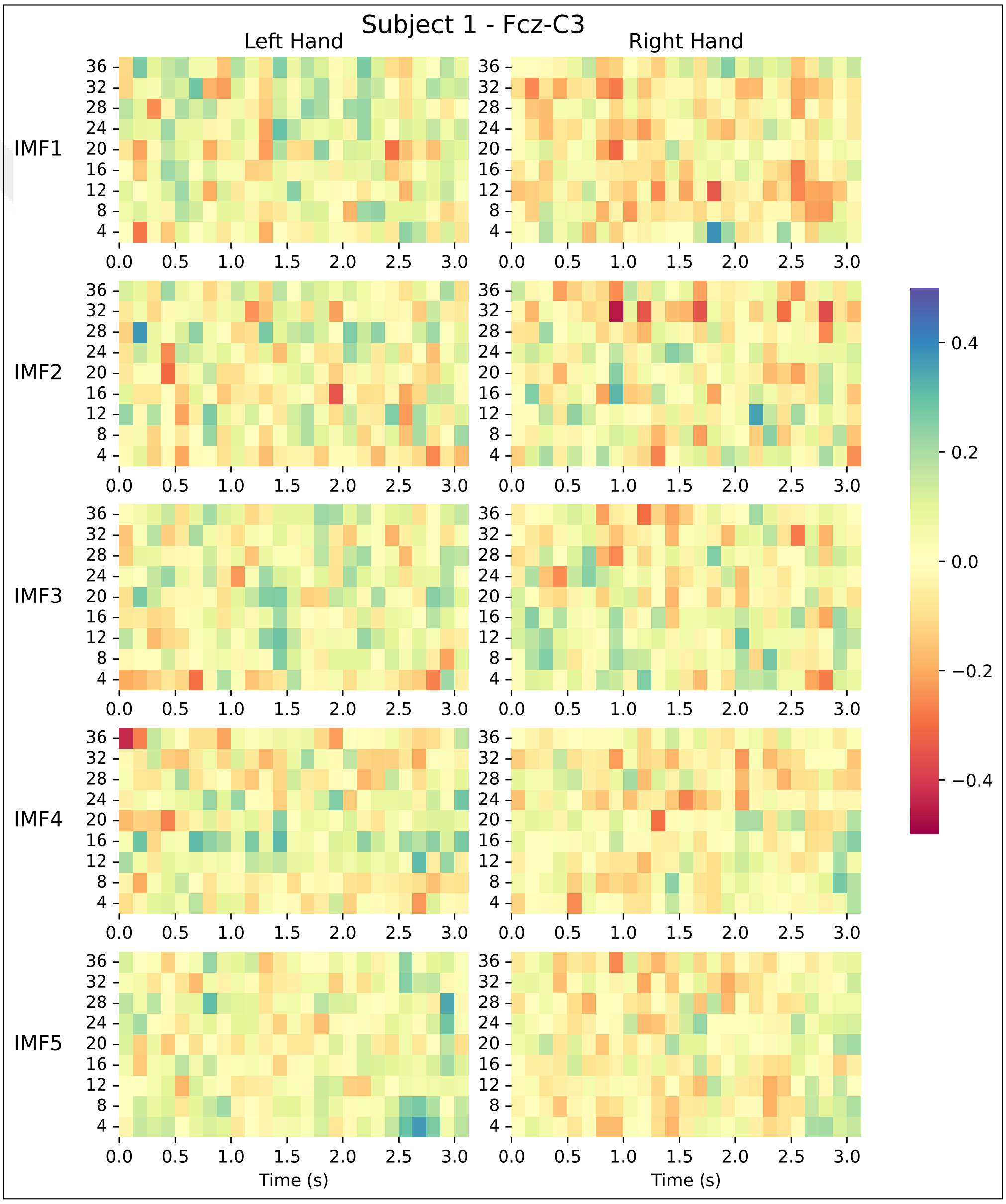

Figure 4.7 Time-frequency plot of $iCOH$ for channels $FCz - C3$.

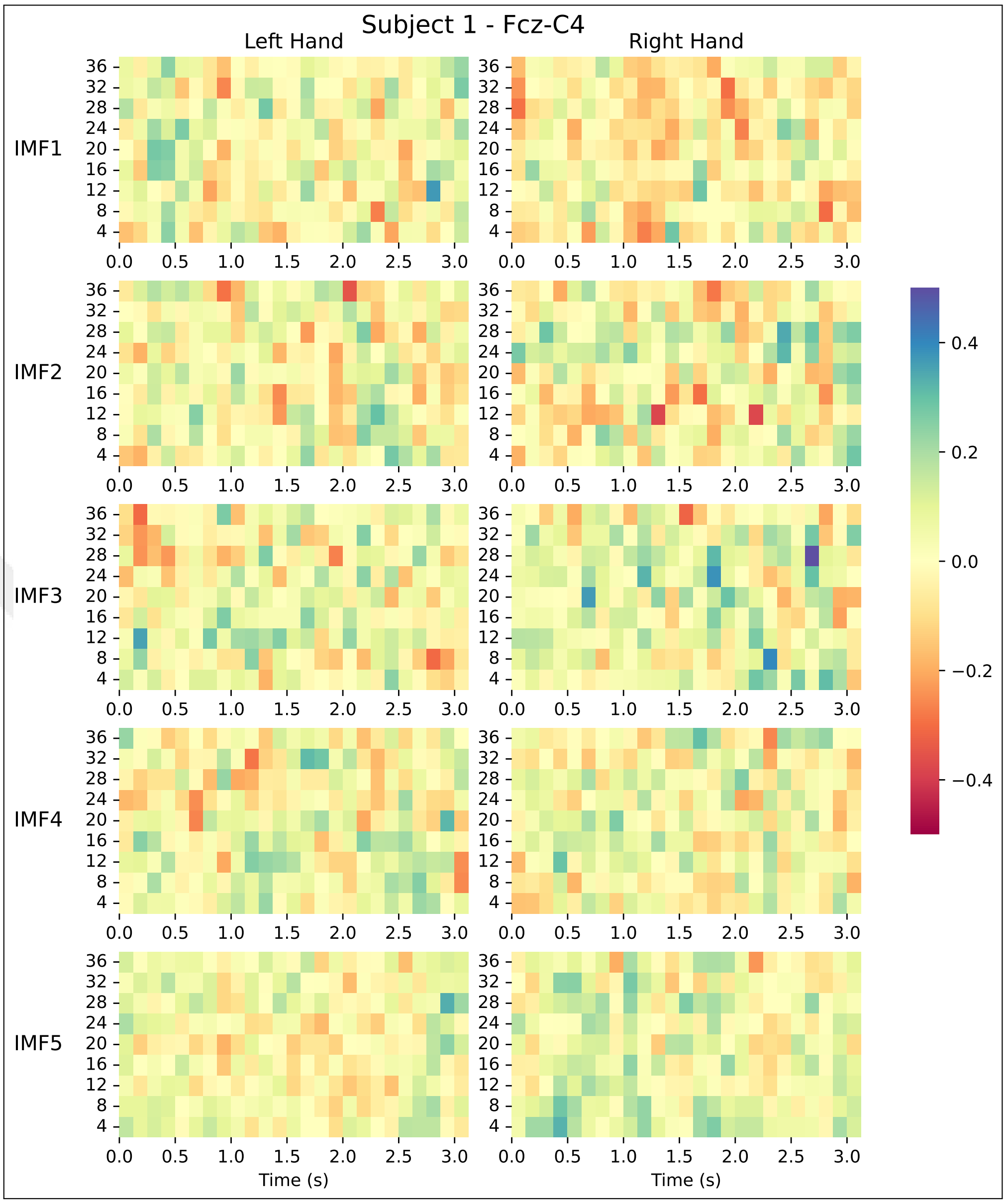

Figure 4.8 Time-frequency plot of $iCOH$ for channels $FCz - C4$.

4.4 Motor imagery classification

Model training for the classification task is done using *Scikit-learn* module in *Python* programming language. Subject-pooling and within-subject training schemes utilize five-fold cross validation to test the generalizability of the models. The models tested in this study are logistic regression, support vector machine, linear discriminant analysis, random forest classifier, and gradient boosting classifier. The base models provided in the *Scikit-learn* package are used for training and further hyperparameter tuning was not done.

4.4.1 Basic IMF features

Subject-pooling scheme is used to test the usability of basic statistical descriptors as features for motor imagery classification. Table 4.1 shows the classification results for each classifier.

Table 4.1
Classification results for each classifier using basic IMF features.

	Logistic Regression	SVM	LDA	Random Forest	GBC
Mean	0.50	0.50	0.54	0.51	0.52
Std.Dev.	0.01	0.01	0.02	0.02	0.01
Min	0.48	0.49	0.51	0.48	0.50
Max	0.52	0.51	0.56	0.54	0.53

4.4.2 Phase locking value

The general performance of single-trial PLV features were tested using subject-pooling. Table 4.2 shows the classification results for each classifier using PLV features.

Table 4.2
Classification results for each classifier using single-trial PLV features.

	Logistic Regression	SVM	LDA	Random Forest	GBC
Mean	0.52	0.50	0.51	0.51	0.51
Std.Dev.	0.01	0.01	0.01	0.03	0.01
Min	0.51	0.49	0.50	0.47	0.50
Max	0.53	0.52	0.52	0.53	0.53

4.4.3 Coherence

Models are trained using single-trial COH features with subject-pooling in order to test the usability of COH for motor imagery task identification. Classification results for each classifier are given in Table 4.3.

Table 4.3
Classification results for each classifier using trial-based coherence features.

	Logistic Regression	SVM	LDA	Random Forest	GBC
Mean	0.53	0.53	0.54	0.52	0.53
Std.Dev.	0.02	0.02	0.02	0.01	0.01
Min	0.51	0.51	0.51	0.50	0.52
Max	0.55	0.55	0.55	0.53	0.54

4.4.4 Raw data $iCOH$

$iCOH$ features calculated as raw data are first used in subject-pooling scheme to test the general usability of the features. Table 4.4 shows the classification results for each classifier.

Table 4.4
Classification results for each classifier using trial-based imaginary part of coherency features with cross validation.

	Logistic Regression	SVM	LDA	Random Forest	GBC
Mean	0.50	0.50	0.52	0.51	0.51
Std.Dev.	0.01	0.01	0.01	0.02	0.03
Min	0.49	0.49	0.51	0.49	0.49
Max	0.52	0.52	0.53	0.53	0.56

Within-subject training is used to determine the performance of the features for each subject. Table 4.5 shows the overall performance of each classifier across subjects.

Table 4.5
Classification results for each classifier using trial-based imaginary part of coherency features with within-subject training.

	Logistic Regression	SVM	LDA	Random Forest	GBC
Mean	0.51	0.50	0.50	0.50	0.50
Std.Dev.	0.09	0.11	0.09	0.09	0.09
Min	0.30	0.24	0.27	0.30	0.30
Max	0.73	0.76	0.79	0.71	0.69

Leave-one-subject-out scheme is used to determine the performance for new subjects for the model. Table 4.6 shows the overall performance of each classifier across subjects.

Table 4.6
Classification results for each classifier using trial-based imaginary part of coherency features with leave-one-subject-out training.

	Logistic Regression	SVM	LDA	Random Forest	GBC
Mean	0.50	0.50	0.50	0.50	0.50
Std.Dev.	0.05	0.01	0.05	0.03	0.04
Min	0.35	0.46	0.36	0.40	0.38
Max	0.71	0.53	0.69	0.58	0.62

4.4.5 Time-frequency function of iCOH

Statistical descriptors calculated from time-frequency functions of imaginary coherence are used as features to train classifier models. Table 4.7 shows the classification results for each classifier with subject-pooling scheme.

Table 4.7
Classification results for each classifier using time-frequency function of imaginar part of coherency with five-fold cross validation.

	Logistic Regression	SVM	LDA	Random Forest	GBC
Mean	0.56	0.57	0.56	0.55	0.56
Std.Dev.	0.03	0.02	0.03	0.01	0.02
Min	0.51	0.54	0.32	0.53	0.33
Max	0.59	0.58	0.58	0.56	0.58

Within-subject training scheme is used to determine the performance for each individual subject. Overall classification results with within-subject training is given in Table 4.8.

Table 4.8
Classification results for each classifier using time-frequency function of imaginary part of coherency features with within-subject training.

	Logistic Regression	SVM	LDA	Random Forest	GBC
Mean	0.58	0.57	0.55	0.58	0.58
Std.Dev.	0.12	0.11	0.10	0.12	0.12
Min	0.27	0.27	0.33	0.30	0.35
Max	0.85	0.85	0.80	0.92	0.95

Leave-one-subject-out scheme is used to test the effectiveness of the features with a newly seen subject. Table 4.9 shows the overall performance of the features with leave-one-subject-out scheme.

Table 4.9
Classification results for each classifier using time-frequency function of imaginary part of coherency features with leave-one-subject-out training.

	Logistic Regression	SVM	LDA	Random Forest	GBC
Mean	0.55	0.51	0.56	0.52	0.53
Std.Dev.	0.09	0.04	0.09	0.05	0.08
Min	0.33	0.42	0.36	0.40	0.38
Max	0.81	0.73	0.83	0.74	0.74

In order to determine the effect of included IMF scales, within-subject training is repeated with all possible combinations of IMF scales. Table 4.10 and Table 4.11 shows the best performance for each subject with selected IMFs, and overall performance of the classifiers.

Table 4.10
Best accuracy scores for each subject with subject-level IMF selection.

Subject	Overall	Logistic Regression	SVM	LDA	Random Forest	GBC
1	0.87	0.78	0.87	0.73	0.76	0.76
2	0.83	0.79	0.77	0.83	0.73	0.64
3	0.71	0.69	0.64	0.71	0.62	0.60
4	0.71	0.68	0.69	0.69	0.71	0.62
5	0.70	0.69	0.66	0.69	0.69	0.70
⋮	⋮	⋮	⋮	⋮	⋮	⋮
105	0.58	0.56	0.50	0.58	0.58	0.57
106	0.73	0.73	0.67	0.71	0.69	0.62
107	0.87	0.80	0.71	0.78	0.87	0.87
108	0.85	0.85	0.71	0.74	0.69	0.65
109	0.81	0.69	0.77	0.81	0.74	0.67

Table 4.11
Performance of each classifier with subject-level IMF selection.

	Overall	Logistic Regression	SVM	LDA	Random Forest	GBC
Mean	0.77	0.72	0.70	0.72	0.71	0.71
Std.Dev.	0.08	0.08	0.08	0.07	0.09	0.09
Min	0.56	0.52	0.47	0.55	0.51	0.53
Max	1.00	0.95	0.93	0.91	0.98	1.00

5. DISCUSSION

First analyses were done using basic statistical descriptors derived from IMFs obtained via NA-MEMD. Classification results using these basic features awere around 0.50 and are consistent across different classifiers. In other words, all classifiers performed at chance level with basic IMF features. This means that basic statistical descriptors of IMFs obtained in time-domain do not contain enough information to distinguish between right-hand/left-hand motor imagery. This is consistent with the literature as motor imagery activity is quite subtle and requires more sophisticated methods to reliably detect.

Commonly used feature extraction methods for motor imagery classification include wavelet transform, common spatial patterns, empirical mode decomposition, common spatial patterns, and deep neural networks. Ma et al. employed wavelet transform and sample entropy, and achieved an accuracy score of 0.89 using 2008 Brain-Computer Interface Competition dataset [4]. Park and Chung utilized local region common spatial pattern and achieved accuracy scores of 0.93 on BCI Competition III Dataset IV_A, 0.85 on BCI Competition IV Dataset I, and 0.82 on BCI Competition IV Dataset II_B [17]. Ge et al. used sinusodial-assisted MEMD with CSP and reported 0.80 accuracy on BCI Competition II Dataset III [22]. Fujiwara and Ushiba reported 0.87 accuracy on Physionet EEG Motor Movement/Imagery Dataset using deep residual convolutional neural networks [37]. Connectivity-based analyses were also employed for motor imagery classification. Benzy and Vinod reported 0.64 accuracy with channel-level PLVs calculated in a different frequency band for each subject on their own dataset with 64 channels [38]. Rodrigues et al. achieved 0.70 accuracy on BCI Competition IV Dataset A and 0.60 accuracy on Dataset B using space-time recurrence based connectivity features with 22 channels [39]. Liu et al. combined channel-level PLV features with frequency band energy features and obtained an accuracy score of 0.92 on BCI Competition IV Dataset II_A [40]. Saha et al. utilized single trial coherence for channel selection along with CSP for feature extraction to achieve 0.93 accuracy with 24 channels and 0.67 accuracy with four channels [41].

Using the connectivity metrics calculated from the raw signals of single trials with subject-pooling classification scheme, all metrics gave classification results at chance level. Among the three metrics tested, COH gave slightly better results with 0.54 accuracy using LDA classifier, however its performance was still close to chance level and could not be reliably used for MI classification. The low accuracy in this method might be due to three reasons. First, the number of channels was limited to four that was most commonly used in MI classification in order to keep the number of channels to a minimum for possible real world applications, and connectivity patterns might not be consistent in a small number of channels. Second, this study used MEMD algorithm to decompose EEG signal, and as MEMD was an entirely data-driven method that did not impose constraints on the decomposition process, IMF scale on which connectivity was observed might differ from subject to subject or even trial to trial. Third, connectivity might have been observed between channels in a limited time window during the task and information might be lost when connectivity was calculated using the entire task duration. Features derived from unrelated IMF scales might hinder the separability of two classes. Classification results obtained from within-subject and leave-one-subject-out training done with raw signal iCOH values, while still giving chance level performance on average, showed variability across subjects. This is consistent with the second reason given for low accuracy.

In order to incorporate connectivity change over time, $iCOH$ was calculated as a function of time and frequency. Using the features derived from $t - f$ function of $iCOH$, trainings done with subject-pooling gave accuracy scores consistently higher than chance level. Best performing classifier was SVM with accuracy score of 0.57. Within-subject training with $t - f$ features also gave results consistently better than chance with GBC performing the best with average accuracy of 0.58 and highest accuracy of 0.95 for a single subject. LDA classifier gave the best results with leave-one-subject-out training with 0.83 highest accuracy for a single subject and 0.56 average accuracy. While results obtained from this classification was better than connectivity metrics calculated from the entire task, achieved accuracy scores are not reliable for

MI classification. An issue with using statistical descriptors of $t - f$ functions is that the descriptors cannot capture the timing or the frequency of connectivity changes. However, the results obtained in this study sufficiently demonstrate the superiority of $t - f$ connectivity features over raw data calculations.

In order to test the effect of IMF scales on the classification results, within subject training was repeated with every possible combination of IMF scales. Using selected IMFs for each subject gave the best accuracy results with average scores of 0.72, 0.70, 0.72, 0.71, 0.71 for *logistic regression classifier*, *SVM*, *LDA*, *random forest classifier*, and *GBC*, respectively. Overall average accuracy was obtained as 0.77 when selecting the best IMFs and best classifier for each subject. These results confirm that IMF scales on which connectivity patterns are observed is subject dependent. Each classifier also gave consistent overall scores however different classifiers performed best for different subjects.

Fundamental point of this study is that it is able to achieve comparable results with those in similar studies that used connectivity metrics [38] as features while utilizing connectivity patterns from only four channels. However, as feature extraction steps include MEMD, connectivity calculations on multiple IMF scales in small time windows over the duration of the task, statistical descriptor calculation, and manual IMF selection, the process can become computationally expensive.

6. CONCLUSION AND FUTURE WORK

The main motivation behind this study was to utilize connectivity patterns to correctly identify intended movement in motor imagery tasks. Multiple connectivity metrics were evaluated for motor imagery classification and the best results were obtained with time-frequency functions of imaginary part of coherency. It was shown that connectivity change over time performed better than connectivity calculated using the full task duration. Obtained accuracy scores were comparable to studies in the literature while using only four channels, increasing usability in a real life scenario.

This study could be further improved by utilizing $t-f$ functions in deep learning methods, such as convolutional neural networks, or encoder-decoder systems, such as long short-term memory. These methods could capture transient changes in connectivity and could potentially achieve higher classification scores.

While the results of this study was comparable to those of similar studies using connectivity, they were not found to be satisfactory in motor imagery classification as a whole. Better accuracy scores are reported using combinations of simpler methods such as CSP, WT, and frequency band energies which lead to the conclusion that functional connectivity metrics may be better used in conjunction with other features, or indirectly used to assist different methodologies.

This study has shown that IMF-level connectivity is subject dependent. This analysis can be further extended to trial-level analyses, and an IMF selection method for MEMD-based classification studies can be derived using functional connectivity. Conventional IMF selection methods utilize similarity metrics between IMFs and the original EEG signal. Using connectivity for IMF selection indirectly incorporates functional connectivity to classification task and may improve performance. Furthermore, IMF-level connectivity metrics may be used to construct multi-scale graph signals for graph-based classification which has gained popularity in recent years.

REFERENCES

1. Wolpaw, J. R., N. Birbaumer, D. J. McFarland, G. Pfurtscheller, and T. M. Vaughan, "Brain-computer interfaces for communication and control," *Clinical Neurophysiology*, Vol. 113, no. 6, pp. 767–791, 2002.

2. Hwang, h.-j., S. Kim, S. Choi, and C.-H. Im, "EEG-based brain-computer interfaces: A thorough literature survey," *International Journal of Human-Computer Interaction*, Vol. 29, 12 2013.

3. Mulder, T., "Motor imagery and action observation: Cognitive tools for rehabilitation," *Journal of neural transmission (Vienna, Austria : 1996)*, Vol. 114, pp. 1265–78, 02 2007.

4. Ma, M., L. Guo, K. Su, and D. Liang, "Classification of motor imagery eeg signals based on wavelet transform and sample entropy," in *2017 IEEE 2nd Advanced Information Technology, Electronic and Automation Control Conference (IAEAC)*, pp. 905–910, 2017.

5. Zhang, Y., Y. Wang, G. Zhou, J. Jin, B. Wang, X. Wang, and A. Cichocki, "Multi-kernel extreme learning machine for EEG classification in brain-computer interfaces," *Expert Systems with Applications*, Vol. 96, pp. 302–310, 2018.

6. Lee, D., H.-J. Lee, and S.-G. Lee, "Motor imagery eeg classification method using emd and fft," *Journal of KIISE*, Vol. 41, pp. 1050–1057, 12 2014.

7. De Vico Fallani, F., J. Richiardi, M. Chavez, and S. Achard, "Graph analysis of functional brain networks: practical issues in translational neuroscience," *Philosophical Transactions of the Royal Society B: Biological Sciences*, Vol. 369, no. 1653, p. 20130521, 2014.

8. Cattai, T., S. Colonnese, M.-C. Corsi, D. S. Bassett, G. Scarano, and F. De Vico Fallani, "Phase/amplitude synchronization of brain signals during motor imagery bci tasks," *IEEE Transactions on Neural Systems and Rehabilitation Engineering*, Vol. 29, pp. 1168–1177, 2021.

9. Lotte, F., C. S. Nam, and A. Nijholt, "Introduction: evolution of brain-computer interfaces," 2018.

10. Lotte, F., *Study of Electroencephalographic Signal Processing and Classification Techniques towards the use of Brain-Computer Interfaces in Virtual Reality Applications*. PhD thesis, INSA de Rennes, 2008.

11. van Dokkum, L., T. Ward, and I. Laffont, "Brain computer interfaces for neurorehabilitation - its current status as a rehabilitation strategy post-stroke," *Annals of Physical and Rehabilitation Medicine*, Vol. 58, no. 1, pp. 3–8, 2015. Brain Computer Interfaces (BCIs) / Coordinated by Jacques LuautÃ© and Isabelle Laffont.

12. Liang, S.-F., F.-Z. Shaw, C.-P. Young, D.-W. Chang, and Y.-C. Liao, "A closed-loop brain computer interface for real-time seizure detection and control," in *2010 Annual International Conference of the IEEE Engineering in Medicine and Biology*, pp. 4950–4953, 2010.

13. Decety, J., "The neurophysiological basis of motor imagery," *Behavioural Brain Research*, Vol. 77, no. 1, pp. 45–52, 1996.

14. Munzert, J., B. Lorey, and K. Zentgraf, “Cognitive motor processes: The role of motor imagery in the study of motor representations,” *Brain Research Reviews*, Vol. 60, no. 2, pp. 306–326, 2009.

15. Pfurtscheller, G., and C. Neuper, “Motor imagery activates primary sensorimotor area in humans,” *Neuroscience Letters*, Vol. 239, no. 2, pp. 65–68, 1997.

16. Pfurtscheller, G., and C. Neuper, “Motor imagery and direct brain-computer communication,” *Proceedings of the IEEE*, Vol. 89, no. 7, pp. 1123–1134, 2001.

17. Park, Y., and W. Chung, “Frequency-optimized local region common spatial pattern approach for motor imagery classification,” *IEEE Transactions on Neural Systems and Rehabilitation Engineering*, Vol. 27, no. 7, pp. 1378–1388, 2019.

18. Wu, S.-L., C.-W. Wu, N. R. Pal, C.-Y. Chen, S.-A. Chen, and C.-T. Lin, “Common spatial pattern and linear discriminant analysis for motor imagery classification,” in *2013 IEEE Symposium on Computational Intelligence, Cognitive Algorithms, Mind, and Brain (CCMB)*, pp. 146–151, 2013.

19. Xu, B., L. Zhang, A. Song, C. Wu, W. Li, D. Zhang, G. Xu, H. Li, and H. Zeng, “Wavelet transform time-frequency image and convolutional network-based motor imagery eeg classification,” *IEEE Access*, Vol. 7, pp. 6084–6093, 2019.

20. Xu, B.-G., and A.-G. Song, “Pattern recognition of motor imagery eeg using wavelet transform,” *Journal of Biomedical Science and Engineering*, Vol. 1, no. 1, p. 64, 2008.

21. Xiaojing, G., W. Xiaopei, and Z. Dexiang, “Motor imagery eeg detection by empirical mode decomposition,” in *2008 IEEE International Joint Conference on Neural Networks (IEEE World Congress on Computational Intelligence)*, pp. 2619–2622, 2008.

22. Ge, S., Y.-H. Shi, R.-M. Wang, P. Lin, J.-F. Gao, G.-P. Sun, K. Iramina, Y.-K. Yang, Y. Leng, H.-X. Wang, and W.-M. Zheng, “Sinusoidal signal assisted multivariate empirical mode decomposition for brain-computer interfaces,” *IEEE Journal of Biomedical and Health Informatics*, Vol. 22, no. 5, pp. 1373–1384, 2018.

23. She, Q., Y. Ma, M. Meng, X. Xi, and Z. Luo, “Noise-assisted memd based relevant imfs identification and eeg classification,” *Journal of Central South University*, Vol. 24, pp. 599–608, 2017.

24. Hamedi, M., S. Salleh, and A. Noor, “Electroencephalographic motor imagery brain connectivity analysis for bci: A review,” *Neural Computation*, Vol. 28, pp. 1–43, 05 2016.

25. Demir, A., T. Koike-Akino, Y. Wang, M. Haruna, and D. Erdogmus, “EEG-GNN: graph neural networks for classification of electroencephalogram (EEG) signals,” *CoRR*, Vol. abs/2106.09135, 2021.

26. Goldberger, A. L., L. G. Luis A. N. Amaral, J. M. Hausdorff, P. C. Ivanov, R. G. Mark, J. E. Mietus, G. B. Moody, C.-K. Peng, and H. E. Stanley, “Physiobank, Physiotoolkit, and Physionet: Components of a new research resource for complex physiologic signals,” *Circulation [Online]*, Vol. e215-e220, pp. 1034–1043, 2000.

27. Schalk, G., D. McFarland, T. Hinterberger, N. Birbaumer, and J. Wolpaw, “Bci2000: a general-purpose brain-computer interface (bci) system,” *IEEE Transactions on Biomedical Engineering*, Vol. 51, no. 6, pp. 1034–1043, 2004.

28. Huang, N. E., Z. Shen, S. R. Long, M. C. Wu, H. H. Shih, Q. Zheng, N.-C. Yen, C. C. Tung, and H. H. Liu, "The empirical mode decomposition and the hilbert spectrum for nonlinear and non-stationary time series analysis," *Proceedings of the Royal Society of London. Series A: Mathematical, Physical and Engineering Sciences*, Vol. 454, no. 1971, pp. 903–995, 1998.

29. Mandic, D. P., N. u. Rehman, Z. Wu, and N. E. Huang, "Empirical mode decomposition-based time-frequency analysis of multivariate signals: The power of adaptive data analysis," *IEEE Signal Processing Magazine*, Vol. 30, no. 6, pp. 74–86, 2013.

30. Rehman, N., and D. P. Mandic, "Multivariate empirical mode decomposition," *Proceedings of the Royal Society A: Mathematical, Physical and Engineering Sciences*, Vol. 466, no. 2117, pp. 1291–1302, 2010.

31. ur Rehman, N., and D. P. Mandic, "Filter bank property of multivariate empirical mode decomposition," *IEEE Transactions on Signal Processing*, Vol. 59, no. 5, pp. 2421–2426, 2011.

32. Rubinov, M., and O. Sporns, "Complex network measures of brain connectivity: Uses and interpretations," *NeuroImage*, Vol. 52, no. 3, pp. 1059–1069, 2010. Computational Models of the Brain.

33. Nolte, G., O. Bai, L. Wheaton, Z. Mari, S. Vorbach, and M. Hallett, "Identifying true brain interaction from eeg data using the imaginary part of coherency," *Clinical Neurophysiology*, Vol. 115, no. 10, pp. 2292–2307, 2004.

34. Hamner, B., R. Leeb, M. Tavella, and J. d. R. Millan, "Phase-based features for motor imagery brain-computer interfaces," *Conference proceedings : ... Annual International Conference of the IEEE Engineering in Medicine and Biology Society. IEEE Engineering in Medicine and Biology Society. Conference*, Vol. 2011, pp. 2578–81, 08 2011.

35. Sander, T., A. Bock, S. Leistner, A. KÃ¼hn, and L. Trahms, "Coherence and imaginary part of coherency identifies cortico-muscular and cortico-thalamic coupling," in *2010 Annual International Conference of the IEEE Engineering in Medicine and Biology*, pp. 1714–1717, 2010.

36. Gramfort, A., M. Luessi, E. Larson, D. A. Engemann, D. Strohmeier, C. Brodbeck, R. Goj, M. Jas, T. Brooks, L. Parkkonen, and M. S. Hämäläinen, "MEG and EEG data analysis with MNE-Python," *Frontiers in Neuroscience*, Vol. 7, no. 267, pp. 1–13, 2013.

37. Fujiwara, Y., and J. Ushiba, "Deep residual convolutional neural networks for brain-computer interface to visualize neural processing of hand movements in the human brain," *Frontiers in Computational Neuroscience*, Vol. 16, 2022.

38. Benzy, V., and A. P. Vinod, "Classification of motor imagery hand movement directions from eeg extracted phase locking value features for brain computer interfaces," in *TENCON 2019 - 2019 IEEE Region 10 Conference (TENCON)*, pp. 2315–2319, 2019.

39. Rodrigues, P., C. Filho, and R. e. a. Attux, "Space-time recurrences for functional connectivity evaluation and feature extraction in motor imagery brain-computer interfaces," *Med Biol Eng Comput*, Vol. 57, pp. 1709–1725, 5 2019.

40. Liu, C., Y. Fu, J. Yang, X. Xiong, H. Sun, and Z. Yu, "Discrimination of motor imagery patterns by electroencephalogram phase synchronization combined with frequency band energy," *IEEE/CAA Journal of Automatica Sinica*, Vol. 4, no. 3, pp. 551–557, 2017.

41. Saha, S., K. I. Ahmed, and R. Mostafa, "Wavelet coherence based channel selection for classifying single trial motor imagery," in *2016 9th International Conference on Electrical and Computer Engineering (ICECE)*, pp. 467–470, 2016.